

Influence of Melt-Spinning Parameters on the Structure and Soft Magnetic Properties of $(\text{Fe}_{0.65}\text{Co}_{0.35})_{88}\text{Zr}_7\text{B}_4\text{Cu}_1$ Alloy

D. ARVINDHA BABU, A.P. SRIVASTAVA, B. MAJUMDAR, D. SRIVASTAVA,
and D. AKHTAR

Melt-spun ribbons of $(\text{Fe}_{0.65}\text{Co}_{0.35})_{88}\text{Zr}_7\text{B}_4\text{Cu}_1$ alloy have been prepared at different wheel speeds, namely, 47, 39, 34, and 17 m/s, and subsequently annealed at 773 K (500 °C) under controlled atmosphere. Structural and soft magnetic properties have been evaluated using X-ray diffraction, differential scanning calorimetry, transmission electron microscopy, and vibrating sample magnetometer. The structure of as-spun ribbons changes from fully amorphous to partially amorphous/nanocrystalline to fully nanocrystalline (bcc α -Fe(Co) + Fe_2Zr) on decreasing the wheel speed. Annealing of amorphous ribbons leads to the precipitation of nanocrystalline bcc α -Fe(Co) phase. The Curie temperature (T_c) of the amorphous phase is found to increase with decreasing wheel speed possibly due to the effect of exchange field penetration of nanocrystals present in the amorphous matrix. The saturation magnetization ($4\pi M_s$) of as-spun ribbons having partially nanocrystalline bcc α -Fe(Co) phase is high as compared to the ribbons with completely amorphous phase, and it remains almost the same even after annealing. The lowest coercivity has been achieved in the ribbons that are fully amorphous, and the coercivity was found to increase with decreasing wheel speed.

DOI: 10.1007/s11661-009-0159-9

© The Minerals, Metals & Materials Society and ASM International 2010

I. INTRODUCTION

NANOCRYSTALLINE soft magnetic materials (FINEMET, NANOPERM, and HITPERM), obtained through partial devitrification of amorphous precursor, have been studied extensively because of their superior properties as compared to the conventional soft magnetic alloys. FINEMET (Fe-Si-B-Nb-Cu) alloys, developed by Yoshizawa *et al.*,^[1] and NANOPERM (Fe-Zr-B-Cu) alloys, developed by Suzuki *et al.*,^[2] exhibit very low coercivity (H_c), high permeability (μ), and low losses, which can be used for room-temperature applications such as distribution transformers and sensors. On the other hand, HITPERM (Fe-Co-Zr-B-Cu) alloy, developed by McHenry *et al.*,^[3] possesses higher saturation magnetization ($4\pi M_s$) and Curie temperature (T_c) and can be used for high-temperature applications such as the rotor assembly of an aircraft integrated power unit, which operates at 773 to 873 K (500 to 600 °C).^[4] The alloy has been developed by partial substitution of Fe by Co in NANOPERM alloy, which leads to enhancement of saturation magnetization and Curie temperature at the cost of coercivity and permeability.

Numerous investigations have been carried out to study the effect of composition, alloying addition, heat treatment, *etc.* on the structure and soft magnetic properties of Fe-Co-Zr-B-Cu alloy systems.^[5-9] Willard *et al.*^[5] have investigated the sequence of reaction during annealing treatment of Fe-Co-Zr-B-Cu alloys and reported that α' -FeCo (B2) nanocrystalline phase is precipitated on crystallization. Müller *et al.*^[9] reported, at higher Co content, fcc Co phase precipitates along with α -Fe(Co) phase in $\text{Fe}_{86-x}\text{Co}_x\text{Zr}_7\text{B}_6\text{Cu}_1$ alloys. The T_c of the amorphous phase was also found to increase with Co content, and beyond 20 at. pct Co, it is higher than the crystallization temperature of α -Fe(Co) phase resulting in difficulties of measuring T_c . Johnson *et al.*^[10] have studied the effect of changing the ratio of Fe:Co from 50:50 to 65:35 on the magnetic properties of $(\text{FeCo})_{89}\text{Zr}_7\text{B}_4$ alloys. The alloy of 65:35 was found to possess higher permeability than the alloy of 50:50 because of high saturation magnetization.

Effect of process parameters during melt spinning on the structure and soft magnetic properties of nanocrystalline materials have been studied in Fe-Si-B-Cu-Nb^[11] and Fe-Zr-Nb-B-Cu^[12,13] alloys. In the case of Fe-Si-B-Cu-Nb alloys, Shahri *et al.*^[11] reported that lower wheel speed leads to the deterioration of soft magnetic properties due to the decrease in degree of amorphicity and increase in magnetostriction. In the case of Fe-Zr-Nb-B-Cu alloys, Wu *et al.*^[12] reported that the textured sample shows inferior soft magnetic properties as compared to fully amorphous ribbons. Recently, Arvindha Babu *et al.*^[13] reported that, in Fe-Zr-B-Cu alloy, on decreasing the wheel speed, the structure changes from completely amorphous phase to a cellular structure of bcc solid solution coexisting with the

D. ARVINDHA BABU, Scientist "C," B. MAJUMDAR, Scientist "E," and D. AKHTAR, Scientist "G," are with the Defence Metallurgical Research Laboratory, Hyderabad-500058, India. Contact e-mail: bhaskarmajumdar1@rediffmail.com A.P. SRIVASTAVA, Scientific Officer "D," and D. SRIVASTAVA, Scientific Officer "H," are with the Materials Science Division, Bhabha Atomic Research Centre, Mumbai-400094, India.

Manuscript submitted June 22, 2009.

Article published online February 12, 2010

amorphous phase at the intercellular region. Annealing leads to the precipitation of nanocrystalline bcc-Fe phase from both amorphous phase and already existing bcc solid solution. It was shown that the soft magnetic properties remain the same irrespective of the initial process conditions.

The present investigation aims at understanding the microstructure and soft magnetic properties of amorphous and annealed $(\text{Fe}_{0.65}\text{Co}_{0.35})_{88}\text{Zr}_7\text{B}_4\text{Cu}_1$ alloy melt spun at different wheel speeds. It is shown that, unlike Fe-Zr-B-Cu alloy, the soft magnetic properties of $(\text{Fe}_{0.65}\text{Co}_{0.35})_{88}\text{Zr}_7\text{B}_4\text{Cu}_1$ alloy are drastically altered on decreasing the wheel speed.

II. EXPERIMENTAL

An alloy with nominal composition $(\text{Fe}_{0.65}\text{Co}_{0.35})_{88}\text{Zr}_7\text{B}_4\text{Cu}_1$ was prepared in a vacuum induction melting furnace using premelted Fe-Zr eutectic alloy ingot and elemental Fe, Co, B, and Cu. The alloy was melt spun under controlled Ar atmosphere at different wheel speeds, namely, 47, 39, 34, and 17 m/s. Detailed experimental conditions for the preparation of rapidly solidified ribbons have been reported earlier.^[14] As-spun ribbons were sealed in a quartz tube under vacuum (2×10^{-5} mbar) and annealed at different temperatures (773 K (500 °C) to 873 K (600 °C)) for 1 hour.

Structural characterization of the as-spun and annealed ribbons was carried out using an X-Ray diffractometer (XRD) (PHILIPS* PW1830). Thermal

*PHILIPS is a trademark of Philips Electronic Instruments Corp., Mahwah, NJ.

analysis for crystallization studies was carried out using a differential scanning calorimeter (DSC) (TA Instruments DSC 910S, TA Instruments, New Castle, DE). Microstructural evaluation was carried out using a transmission electron microscope (TEM) (JEOL**

**JEOL is a trademark of Japan Electron Optics Ltd., Tokyo.

2000FX TEM). A precision ion polishing system (PIPS) was employed for TEM sample preparation by thinning from both the sides of the ribbon. Thermomagnetic plots (up to 823 K (550 °C) at a field of 500 Oe) and saturation magnetization ($4\pi M_s$) (at a field of 5 kOe) were obtained using a vibrating sample magnetometer (VSM) (ADE† EV9). Coercivity of as-spun and

†ADE is a trademark of Microsense, LLC, Boston, MA.

annealed ribbons was measured using a Coercimeter (Foerster-Koerzimat 1.095, Institut Dr. Foerster GmbH & Co. KG, Reutlingen, Baden-Wuerttemberg, Germany).

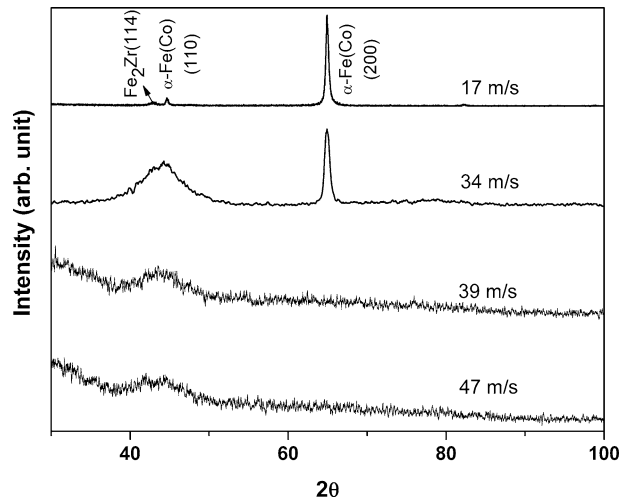


Fig. 1—XRD patterns (Cu K_α radiation) of as-spun ribbons prepared at wheel speeds of 47, 39, 34, and 17 m/s.

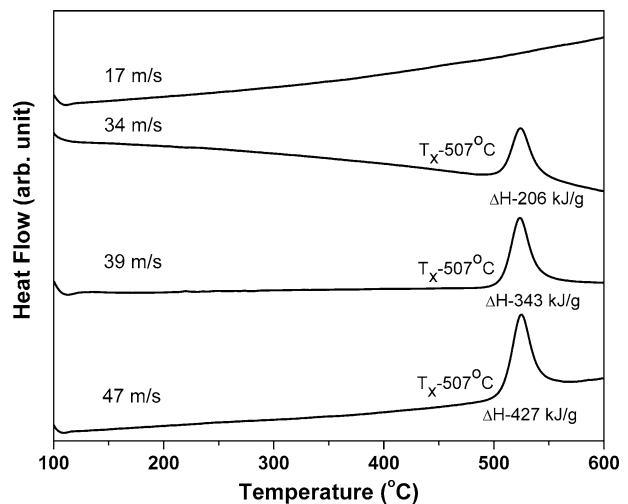


Fig. 2—DSC thermograms (heating rate 20 °C/min) of as-spun ribbons prepared at wheel speeds of 47, 39, 34, and 17 m/s.

III. RESULTS

A. Structure

The average thickness of melt-spun ribbons was found to be 31, 40, 52, and 72 μm for ribbons prepared at the wheel speeds of 47, 39, 34, and 17 m/s, respectively. Figure 1 shows the XRD patterns of ribbons prepared at different wheel speeds. Ribbons prepared at wheel speeds of 47 and 39 m/s are fully amorphous. In the 34 m/s ribbon, the amorphous phase is found to coexist with the bcc α -Fe(Co) phase. A strong reflection from the (200) plane as compared to the reflection from the (110) plane reveals texture along the $\langle 100 \rangle$ direction. On decreasing the wheel speed to 17 m/s, completely crystalline phase (bcc α -Fe(Co) phase) is obtained with a strong texture along the $\langle 100 \rangle$ direction. A small intensity peak appears at $2\theta = 42.8$ deg revealing the formation of Fe_2Zr phase along with bcc α -Fe(Co) phase in these ribbons.

Figure 2 shows the DSC thermograms obtained at a heating rate of 20 °C/min for ribbons prepared at different wheel speeds. Exothermic peaks corresponding to the primary crystallization of amorphous phase are observed for the ribbons processed at wheel speeds of 47, 39, and 34 m/s. It should be noted that the onset of

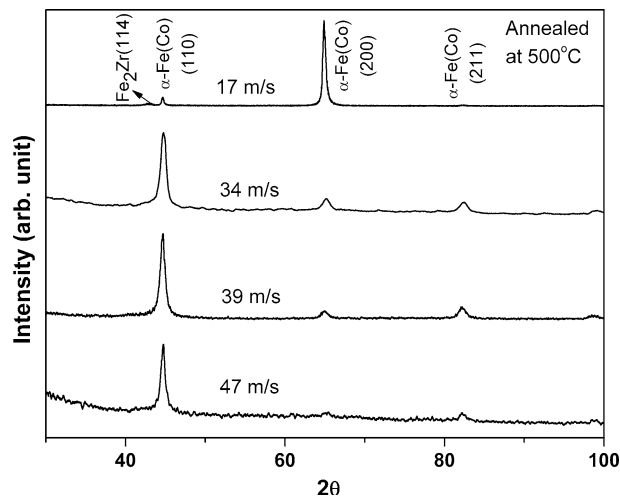


Fig. 3—XRD patterns (Cu K_α radiation) of the ribbons annealed at 773 K (500 °C) for 1 h.

crystallization (T_x) is 780 K (507 °C), which is the same for all ribbons. The enthalpies of crystallization, calculated from the area under the exothermic peaks, are 427, 343, and 206 kJ/g for 47, 39, and 34 m/s ribbons, respectively. No exothermic peak is observed up to 873 K (600 °C) in 17 m/s ribbon, which confirms that the as-spun ribbon is fully crystalline. Figure 3 shows XRD patterns of all ribbons annealed at 773 K (500 °C) temperature for 1 hour revealing the precipitation of bcc α -Fe(Co) phase from amorphous matrix. In the case of 17 m/s ribbon, the texture remains unaffected even after annealing.

Figures 4(a) and (b) show the TEM bright-field (BF) images of as-spun and annealed ribbons prepared at the wheel speed of 47 m/s, respectively. The featureless contrast and the corresponding halo ring in the selected area diffraction (SAD) pattern (Figure 4(a)) indicate that as-spun ribbon is completely amorphous. The average composition obtained from electron diffraction X-ray (EDAX) analysis is Fe: 55.1, Co: 30.9, Zr: 9.7, and Cu: 4.3 at. pct. It should be noted that B could not be detected through EDAX probe. Annealing leads to the formation of nanocrystals of bcc α -Fe(Co) phase (Figure 4(b)). The grain size (D_g) was measured from both TEM BF and dark-field (DF) images in an area of 500 nm \times 600 nm for about 100 to 200 grains. Details of the measurement technique can be found elsewhere.^[15] Figure 4(c) shows the histogram for

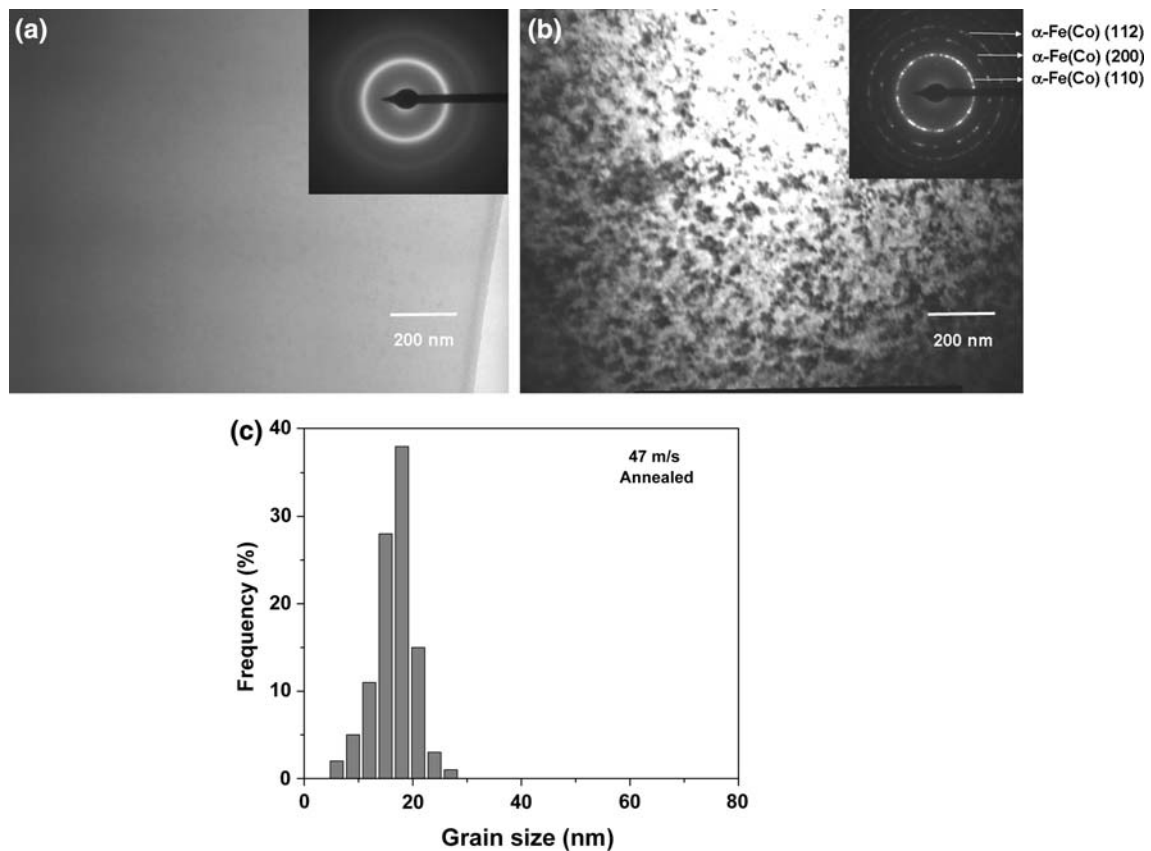


Fig. 4—Transmission electron microscopy of 47 m/s ribbons: (a) BF image of as-spun ribbon (inset is SAD pattern), (b) BF image of 773 K (500 °C) annealed ribbon (inset is SAD pattern), and (c) histogram of 773 K (500 °C) annealed ribbon.

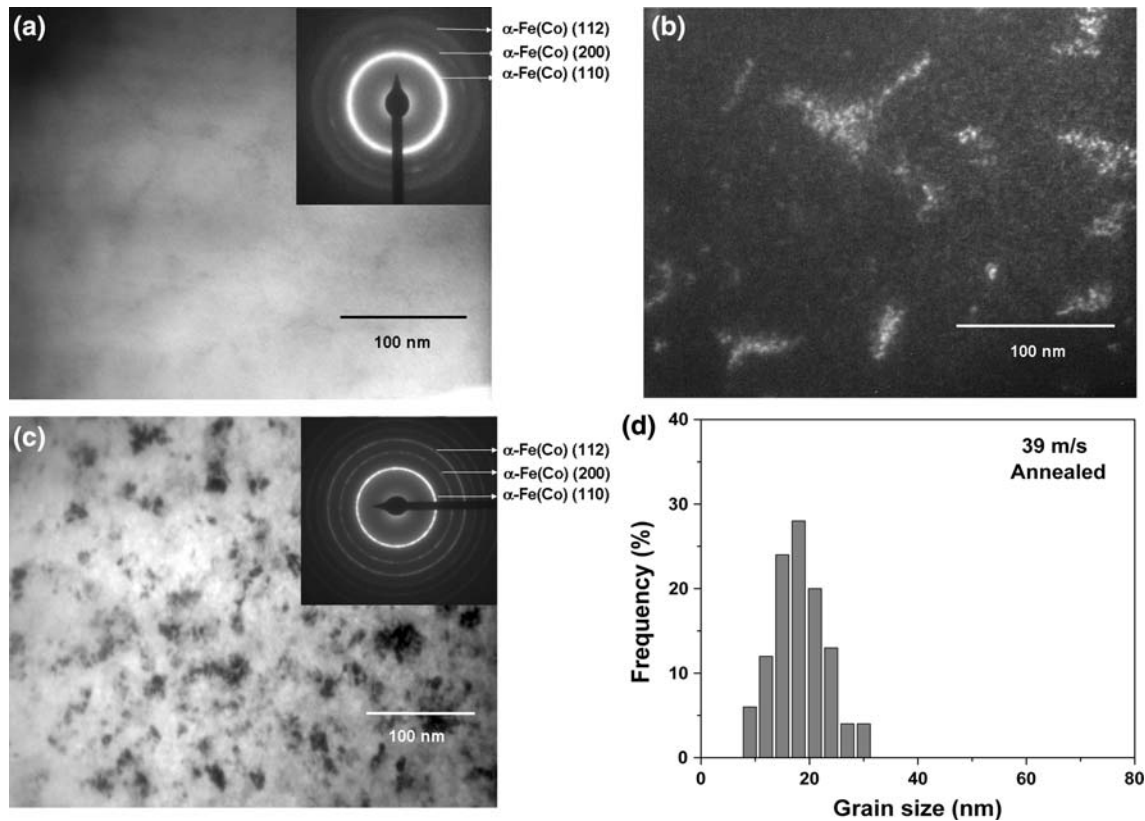


Fig. 5—Transmission electron microscopy of 39 m/s ribbons: (a) BF image of as-spun ribbon (inset is SAD pattern), (b) DF image of as-spun ribbon, (c) BF image of 773 K (500 °C) annealed ribbon (inset is SAD pattern), and (d) histogram of 773 K (500 °C) annealed ribbon.

773 K (500 °C) annealed ribbon revealing a narrow distribution of grain size.

Figure 5 shows the (a) TEM BF and (b) DF images of the as-spun and (c) BF image of 773 K (500 °C) annealed ribbons prepared at the wheel speed of 39 m/s. Insets in the BF images show the SAD patterns. It is interesting to note that clusters of nanocrystallites (whose size in the range of 1 to 3 nm) can be observed along with the amorphous phase in the DF image of as-spun ribbon (Figure 5(b)), which could not be detected in the BF image as well as in the XRD pattern (Figure 1). The composition of the amorphous phase obtained from EDAX analysis is Fe: 57.3, Co: 29.3, Zr: 7.4, and Cu: 6.0 at. pct. The (200) and (112) reflections in the SAD pattern (inset in Figure 5(a)) confirm the existence of the nanocrystalline bcc Fe(Co) phase. Annealing at 773 K (500 °C) leads to the coarsening of existing nanocrystalline phase and formation of new nanocrystals from the amorphous phase (Figure 5(c)). Figure 5(d) shows the histogram of grain size distribution revealing that the grains are spread between 9 and 31 nm.

Figures 6(a) and (c) show the TEM BF image of as-spun ribbon prepared at the wheel speed of 34 m/s and corresponding grain size distribution, respectively. It is interesting to note the formation of α -Fe(Co) nanocrystalline phase along with amorphous phase in the as-spun condition. The EDAX analysis revealed that

the composition of the amorphous region is Fe: 56.2, Co: 31.4, Zr: 8.4, and Cu: 3.8 at. pct. The grain size distribution (Figure 6(c)) is narrow. Figure 6(b) shows the TEM BF image of the same ribbon annealed at 773 K (500 °C) temperature revealing that the density of the nanograins increases as compared to as-spun condition. Figure 6(d) shows the grain size distribution of the preceding ribbon.

The morphology of the as-spun and annealed ribbons prepared at the wheel speed of 17 m/s are shown in Figure 7. Figures 7(a) and (b) show the TEM BF images, whereas Figures 7(c) and (d) show the corresponding grain size distribution of as-spun and annealed ribbons, respectively. The indexing of SAD patterns indicates the formation of nanocrystalline Fe_2Zr along with α -Fe(Co) phase. It can be observed from Figures 7(c) and (d) that the grain size exhibits bimodal distributions in the as-spun and annealed conditions.

B. Magnetic Properties

Figure 8 shows the thermomagnetic curves of different as-spun ribbons up to 823 K (550 °C) measured at a field of 500 Oe. The ferro- to paramagnetic transition (Curie temperature, T_c) of the amorphous phase is found to be 723 K (450 °C), 731 K (458 °C), and 796 K (523 °C) for the ribbons prepared at the wheel speeds of 47, 39, and 34 m/s, respectively. In the case of

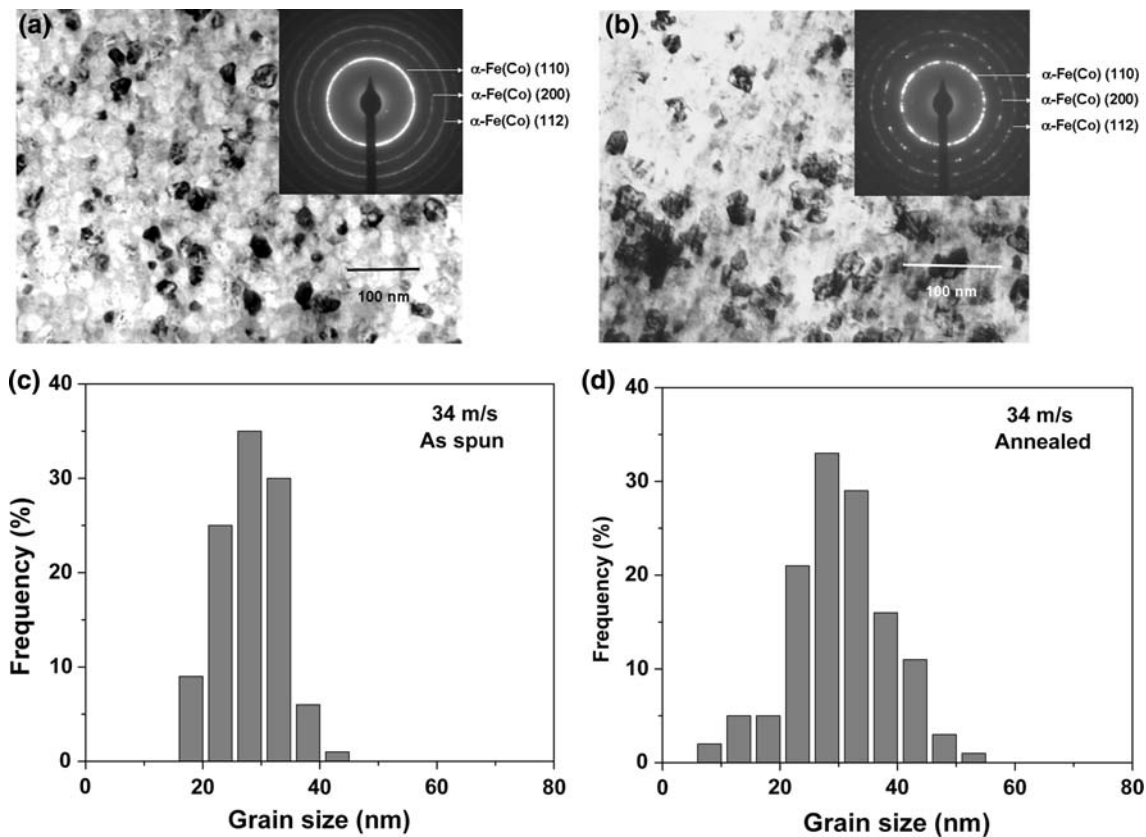


Fig. 6—Transmission electron microscopy of 34 m/s ribbons: (a) BF image of as-spun ribbon (inset is SAD pattern), (b) BF image of 773 K (500 °C) ribbon (inset is SAD pattern), (c) histogram of as-spun ribbon, and (d) histogram of 773 K (500 °C) annealed ribbon.

the 17 m/s ribbon, which consists of only nanocrystalline phases, the magnetization decreases monotonously and no T_c is observed until 823 K (550 °C). Figure 9 shows the variation of room-temperature saturation magnetization ($4\pi M_s$) with annealing temperature measured at 5 kOe for the ribbons prepared at different wheel speeds. The $4\pi M_s$ values of as-spun ribbons are also indicated on the abscissa. It can be observed that the $4\pi M_s$ of as-spun ribbons increases on decreasing the wheel speed.

Figure 10 shows the dependence of coercivity on annealing temperature for the ribbons prepared at different wheel speeds. The coercivity of as-spun ribbons is also indicated on the abscissa. In the case of 47, 39, and 34 m/s specimens, the coercivity remains almost the same for the as-spun and annealed conditions. Coercivity values of 47 and 39 m/s ribbons are in the range of 0.23 to 0.25 Oe, whereas the coercivity value increases slightly (0.37 to 0.39 Oe) for 34 m/s ribbon. In the case of the 17 m/s ribbon, the coercivity of the as-spun ribbon is an order of magnitude higher (2.7 Oe) and it further increases on annealing.

IV. DISCUSSION

Our results indicate that the structure of melt-spun ($\text{Fe}_{0.65}\text{Co}_{0.35}$)₈₈Zr₇B₄Cu₁ ribbons changes from completely amorphous to partially nanocrystalline (α -Fe(Co)

phase) and then to fully nanocrystalline (α -Fe(Co) and Fe_2Zr phases) on decreasing the wheel speed from 47 to 17 m/s. The decrease in enthalpy of crystallization with the decrease of wheel speed also indicates that the amount of amorphous phase reduces with wheel speed. Finally, no crystallization peak is observed in 17 m/s ribbon because of the absence of amorphous phase.

Amorphous phase formation occurs if the alloy can be undercooled below the glass transition temperature without crystallization.^[16] Such high undercooling is achieved by suppressing the nucleation of the crystalline phase above a critical cooling rate, bypassing the nose of the temperature-time-transformation (TTT) curve for homogeneous nucleation. In the case of ($\text{Fe}_{0.65}\text{Co}_{0.35}$)₈₈Zr₇B₄Cu₁ alloy, the wheel speed as high as 47 m/s provides the desired critical cooling rate and the alloy becomes completely amorphous. At moderate wheel speeds, *i.e.*, 39 and 34 m/s, the nanocrystalline α -Fe(Co) nucleates as a primary phase and coexists with the amorphous phase. The formation of primary phase in amorphous matrix during intermediate cooling is a well-known phenomenon and has already been reported.^[12]

Although the alloy represents a multicomponent system, the composition of the alloy can be considered as a near eutectic in binary Fe-Zr phase diagram where Co forms bcc solid solution with Fe, and Zr as well as B promotes the formation of intermetallic compound.

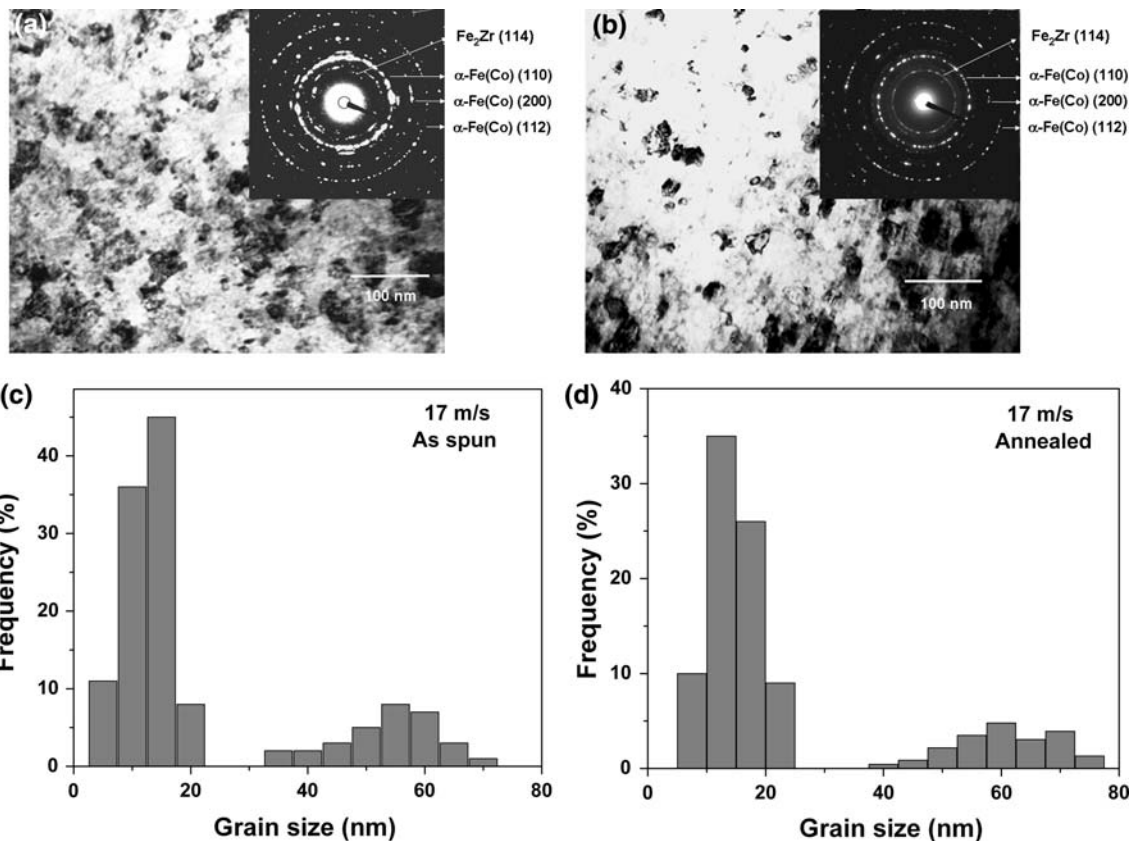


Fig. 7—Transmission electron microscopy of 17 m/s ribbons: (a) BF image of as-spun ribbon (inset is SAD pattern), (b) BF of 773 K (500 °C) ribbon (inset is SAD pattern), (c) histogram of as-spun ribbon, and (d) histogram of 773 K (500 °C) annealed ribbon.

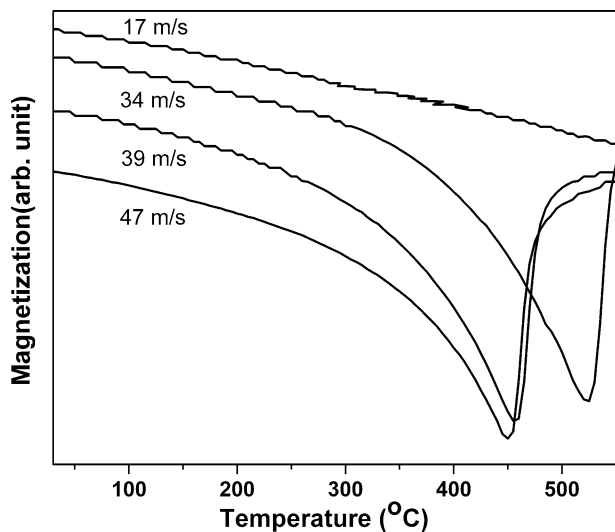


Fig. 8—Thermomagnetic curves (500 Oe) of ribbons prepared at wheel speeds of 47, 39, 34, and 17 m/s.

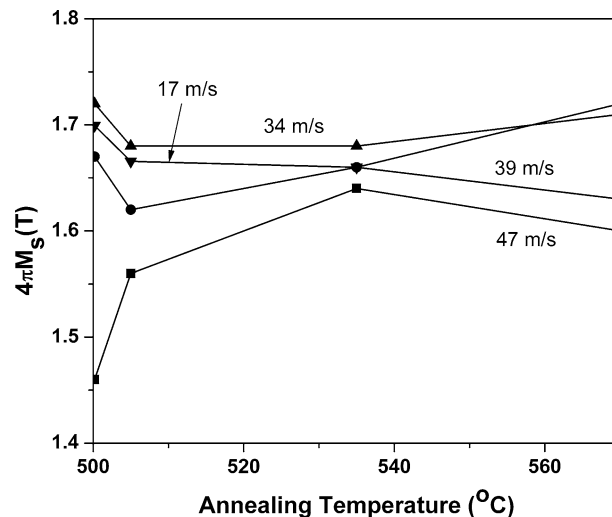


Fig. 9—Variation of saturation magnetization with annealing temperature for different wheel speed ribbons.

Therefore, at lower wheel speed (17 m/s), when the cooling rate is not enough to form glass, eutectic solidification takes place, resulting in simultaneous decomposition of nanocrystalline bcc α -Fe(Co) and Fe_2Zr phases from the melt.^[17]

All histograms of grain size distribution estimated from TEM micrographs were fitted with the Lorentz curve. Data obtained from the analyses of the histograms (average grain size, center of the histogram, and full-width at half-maximum (FWHM)) and the minimum and maximum grain size are given in Table I.

It can be observed that the average grain size of the annealed specimens increases with decreasing wheel speed. The FWHM has also increased on decreasing the wheel speed, indicating that the scatter in grain size increases with the reduction of cooling rate. In the case of 17 m/s ribbon, the histograms could be fitted with two distribution curves for both as-spun and annealed ribbons. The first curve (smaller grain size) of as-spun ribbon shows the average grain size of 9.9 nm with the FWHM of 9.77 nm, which is even smaller than the grain size of the annealed specimen prepared at higher wheel speed. The second curve shows the average grain size of 52 nm with the FWHM of 13.2 nm. These grains are larger than that of the annealed specimen prepared at higher wheel speed. Considering the frequency distribution and XRD results, the larger grains may be attributed to the Fe₂Zr phase.

It is reported that in this type of alloys, α -Fe(Co) particles do not show appreciable growth during solidification or during annealing treatment.^[15] Our results are consistent with the preceding observation as the average size of α -Fe particles is nearly the same/slightly increased for both as-spun and annealed conditions. However, the growth of Fe₂Zr phase is dependent on solidification time. Therefore, in the case of 17 m/s

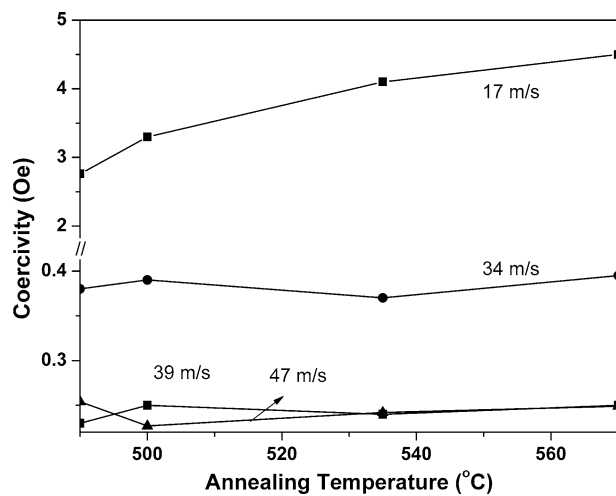


Fig. 10—Variation of coercivity with annealing temperature for different wheel speed ribbons.

ribbon, as soon as the Fe₂Zr starts forming, it grows faster than α -Fe. The growth of α -Fe is further retarded in the presence of Fe₂Zr.

The Curie temperature (T_c) of amorphous phase is found to increase with the decreasing wheel speed. Detailed EDAX analyses of 47, 39, and 34 m/s ribbons have revealed that the composition of amorphous phase is almost the same irrespective of whether the as-spun ribbon is fully amorphous or partially crystalline (within the experimental errors of EDAX results). Moreover, the temperature of the onset of crystallization for all the ribbons observed from the DSC thermograms is also the same, which supports the uniformity of the amorphous phase compositions for all ribbons. The increases of T_c of the amorphous phase with decreasing wheel speed, therefore, can be attributed to the effect of exchange field penetration of the nanocrystalline phase formed during melt spinning within the amorphous matrix at lower wheel speed.^[18,19]

The increase of saturation magnetization on decreasing the wheel speed is due to the precipitation of nanocrystalline α -Fe(Co) phase, which has a higher saturation magnetization value as compared to the amorphous phase.^[3] A lower saturation in as-spun 17 m/s ribbon can be attributed to the formation of Fe₂Zr phase. The increase in the $4\pi M_s$ value of 47 m/s ribbon on annealing is also due to the formation of nanocrystalline α -Fe(Co) phase. In the case of 39, 34, and 17 m/s ribbons, the $4\pi M_s$ values decrease slightly and then remain almost the same with increasing annealing temperature. The initial decrease of the saturation is attributed to the increase of Zr/B concentration in the precipitate phase.

The behavior of the coercivity of Fe-Co-Zr-B-Cu alloy with annealing temperature is different from that of Fe-Si-B-Nb-Cu^[11] and Fe-Zr-B-Cu^[13] alloys. Low coercivity is achieved in 47 and 39 m/s ribbons, which are fully/almost amorphous, and annealing has no significant effect on the coercivity. In nanocrystalline soft magnetic materials, the magnetic properties depend on the size and distribution of nanocrystalline grains in amorphous matrix. Under the application of magnetic field, exchange coupling between nanocrystals and amorphous phase takes place, leading to averaging out of the magnetocrystalline anisotropy (K_1), and the exchange interaction forces the magnetization vector

Table I. Grain Size Distribution Obtained from Lorentz Fitting of Histogram

Wheel speed (m/s)	Condition	Phase	Minimum Grain Size (nm)	Maximum Grain Size (nm)	Average Grain Size (D_g) (nm)	Center (nm)	FWHM (nm)
47	as spun	—	—	—	—	—	—
	annealed	α -Fe	4.9	28.1	19	17.13	7.45
39	as spun	—	—	—	—	—	—
	annealed	α -Fe	9.2	31	20	18	15.72
34	as spun	α -Fe	17	41.5	26	28.30	19.63
	annealed	α -Fe	7.3	53	30	29.92	16.79
17	as spun	α -Fe	5.1	17.4	9.9	10.15	9.77
	annealed	Fe ₂ Zr	30.6	69.8	52	56.04	13.24
		α -Fe	7.2	22.7	12	13.58	11.7
		Fe ₂ Zr	40.3	76.2	58	61.38	34.4

to be aligned over several grains along the field direction.^[20] In the framework of the Alben theory of the random anisotropy model, Herzer^[21] gave the relation between coercivity (H_c) with grain size (D_g) below the exchange length as

$$H_c = \frac{p_c K_1 D_g^6}{J_s A^3}$$

where A stands for the exchange stiffness, J_s is the exchange energy, and p_c is the magnetic moment. It is evident that the increase of coercivity for 34 m/s ribbon is due to the increase of the grain size (D_g) of nanocrystalline phase. The presence of texture also can be attributed to the increase of coercivity.^[12] The soft magnetic properties deteriorate abruptly due to the formation of magnetically hard nanocrystalline Fe₂Zr phase along with Fe(Co) phase (texture along $\langle 100 \rangle$) in as-spun 17 m/s ribbon, and the coercivity increases by an order of magnitude.

V. CONCLUSIONS

1. The structure of melt-spun ribbons of (Fe_{0.65}-Co_{0.35})₈₈Zr₇B₄Cu₁ alloy changes from completely amorphous to partially amorphous/nanocrystalline and then fully nanocrystalline (bcc α -Fe(Co) + Fe₂Zr) on decreasing the wheel speed.
2. Annealing leads to the precipitation of nanocrystalline bcc-Fe(Co) phase in the amorphous matrix. The grain size of 17 m/s ribbon exhibits a bimodal distribution in the as-spun and annealed conditions.
3. The T_c of amorphous phase increases with decreasing wheel speed due to the effect of exchange field penetration of nanocrystalline phase increasingly present in the amorphous matrix.
4. The saturation magnetization ($4\pi M_s$) value of as-spun ribbons having bcc α -Fe(Co) phase is high as compared to the ribbons with completely amorphous phase.
5. Coercivity is the same for as-spun and annealed ribbons of 47 and 39 m/s wheel speed and increases to higher values for lower wheel speeds due to the increase in average grain size/absence of amorphous matrix.

ACKNOWLEDGMENTS

This work was supported by the Defence Research and Development Organization (DRDO), New Delhi,

India. The authors thank Dr. A.K. Singh, DMRL, Hyderabad, India, and Dr. Kiran, MIDHANI, Hyderabad, India, for their help with XRD and coercivity measurements. It is a pleasure to thank Dr. G. Malakondaiah, Director, DMRL, Hyderabad, India, for continued support and permission to publish this work.

REFERENCES

1. Y. Yoshizawa, S. Oguma, and K. Yamauchi: *J. Appl. Phys.*, 1988, vol. 64, pp. 6044–46.
2. K. Suzuki, A. Makino, N. Kataoka, A. Inoue, and T. Masumoto: *Mater. Trans. JIM*, 1991, vol. 32, pp. 93–102.
3. M.E. McHenry, M.A. Willard, and D.E. Laughlin: *Prog. Mater. Sci.*, 1999, vol. 44, pp. 291–433.
4. B.D. Cullity and C.D. Graham: *Introduction to Magnetic Materials*, John Wiley & Sons, Inc., Hoboken, NJ, 2009, pp. 466–67.
5. M.A. Willard, M.Q. Huang, D.E. Laughlin, M.E. McHenry, J.O. Cross, V.G. Harris, and Franchetti: *J. Appl. Phys.*, 1999, vol. 85, pp. 4421–23.
6. M.A. Willard, D.E. Laughlin, M.E. McHenry, D. Thomas, K. Sickafus, J.O. Cross, and V.G. Harris: *J. Appl. Phys.*, 1998, vol. 84, pp. 6773–77.
7. M.E. McHenry and D.E. Laughlin: *Acta Mater.*, 2000, vol. 48, pp. 223–38.
8. M.A. Willard, D.E. Laughlin, and M.E. McHenry: *J. Appl. Phys.*, 2000, vol. 87, pp. 7091–96.
9. M. Müller, H. Grahl, N. Mattern, U. Kühn, and B. Schnell: *J. Magn. Magn. Mater.*, 1996, vol. 160, pp. 284–86.
10. F. Johnson, C.Y. Um, M.E. McHenry, and H. Garmestani: *J. Magn. Magn. Mater.*, 2008, vol. 297, pp. 93–98.
11. F. Shahri and A. Beitollahi: *J. Non-Cryst. Solids*, 2007, vol. 354, pp. 1487–93.
12. Y.Q. Wu, T. Bitoh, K. Hono, A. Makino, and A. Inoue: *Acta Mater.*, 2001, vol. 49, pp. 4069–77.
13. D. Arvindha Babu, B. Majumdar, R. Sarkar, D. Akhtar, and V. Chandrasekaran: *J. Phys. D: Appl. Phys.*, 2008, vol. 41, pp. 195002–195008.
14. B. Majumdar and D. Akhtar: *Bull. Mater. Sci.*, 2005, vol. 28, pp. 395–99.
15. B. Majumdar, S. Bysak, and D. Akhtar: *J. Magn. Magn. Mater.*, 2007, vol. 309, pp. 300–06.
16. F.E. Luborsky: *Amorphous Metallic Alloys, Monographs in Materials*, Butterworth & Co. Publishers Ltd., London, 1983, pp. 8–11.
17. D. Arias and JP Abriata: *Bull. Alloy Phase Diagrams*, 1988, vol. 9 (5), pp. 597–604.
18. A. Hernando and I. Navarro: *Phys. Rev. B*, 1995, vol. 51, pp. 3281–84.
19. J.S. Garitaonandia, D.S. Schmool, and J.M. Barandiran: *Phys. Rev. B*, 1998, vol. 58, pp. 12147–58.
20. R. Alben, J.J. Becker, and M.C. Chi: *J. Appl. Phys.*, 1978, vol. 47, pp. 1653–58.
21. G. Herzer: *Mater. Sci. Eng.*, 1991, vol. A133, pp. 1–5.